

# Transport evidence of surface states in magnetic topological insulator $\text{MnBi}_2\text{Te}_4$

Michael Wissmann,<sup>1,2</sup> Romain Giraud,<sup>1,2</sup> Börge Mehlhorn,<sup>1,3</sup> Maxime Leroux,<sup>4</sup> Mathieu Pierre,<sup>4</sup> Michel Goiran,<sup>4</sup> Walter Escoffier,<sup>4</sup> Bernd Büchner,<sup>1,3,5</sup> Anna Isaeva,<sup>6,7</sup> Joseph Dufouleur,<sup>1,3</sup> and Louis Veyrat<sup>1,3,4</sup>

<sup>1</sup>*Leibniz Institute for Solid State and Materials Research,  
IFW Dresden, Helmholtzstrasse 20, 01069 Dresden, Germany*

<sup>2</sup>*Université Grenoble Alpes, CNRS, CEA, Grenoble-INP, Spintec, 38000 Grenoble, France*

<sup>3</sup>*Würzburg-Dresden Cluster of Excellence ct.qmat, 01062 Dresden, Germany*

<sup>4</sup>*CNRS, Laboratoire National des Champs Magnétiques Intenses, Université Grenoble-Alpes,  
Université Toulouse 3, INSA-Toulouse, EMFL, 31400 Toulouse, France*

<sup>5</sup>*Department of Physics, TU Dresden, 01062 Dresden, Germany*

<sup>6</sup>*Institute of Physics, University of Amsterdam, 1098 XH Amsterdam, The Netherlands*

<sup>7</sup>*Faculty of Physics, Technical University of Dortmund, 44227 Dortmund, Germany and  
Research Center "Future Energy Materials and Systems" (RC FEMS), 44227, Dortmund, Germany*

(Dated: December 4, 2025)

Magnetic topological insulators can host chiral 1D edge channels at zero magnetic field, when a magnetic gap opens at the Dirac point in the band structure of 2D topological surface states, leading to the quantum anomalous Hall effect in ultra-thin nanostructures. For thicker nanostructures, quantization is severely reduced by the co-existence of edge states with other quasi-particles, usually considered as bulk states. Yet, surface states also exist above the magnetic gap, but it remains difficult to identify electronic subbands by electrical measurements due to strong disorder. Here we unveil surface states in  $\text{MnBi}_2\text{Te}_4$  nanostructures, using magneto-transport in very-high magnetic fields up to 55 T, giving evidence of Shubnikov-de-Haas oscillations above 40 T. A detailed analysis confirms the 2D nature of these quantum oscillations, thus establishing an alternative method to photoemission spectroscopy for the study of topological surface states in magnetic topological insulators, using Landau level spectroscopy.

Topological insulators have metallic interface states at their boundaries, which can be either surface states for 3D systems, or edge states for 2D systems [1–3]. These states are of great interest for applications in spintronics due to their helical spin textures with spin-momentum locking [4, 5], and they are weakly scattered by disorder. In non-magnetic 3D topological insulators, the anisotropic scattering of topological surface states (TSS) results in an increase of their backscattering length, as compared to other quasi-particles, which is associated to the enhanced transport mobility of TSS with respect to the mobility of bulk carriers [6] and which is at the origin of quasi-ballistic transport in narrow quantum wires [7–9]. In magnetic topological insulators, a small non-trivial gap opens in the 2D band structure of surface states due to the exchange field, and 1D ballistic edge states contribute to the quantum anomalous Hall effect [10]. However, the quantization of the transverse resistance in ultra-thin structures, important for quantum metrology [11, 12], can be severely reduced by bulk carriers [13]. Actually, in thicker nanostructures, a major limitation to have quantized transport properties could rather come from surface electronic states, which exist above the magnetic gap but within the bulk-band gap. However, due to strong disorder in magnetic TIs, it remains difficult to evidence the nature of electronic subbands by electrical measurements.

One convenient way to individually access the doping and energy levels of the surface and bulk electronic populations is to perform Landau level spectroscopy. The

measurement of Shubnikov-de-Haas oscillations (SdHO) of the resistance under external magnetic field can give access to the carrier density, the transport and the quantum mobilities, the effective mass and the chemical potential of different charge carrier populations, whose contributions to the total conductance can be disentangled so. However, this technique requires magnetic fields such that  $\mu B > 1$ ,  $\mu$  being the charge carrier mobility, different for each band. While such quantum oscillations have been studied in Sb-doped  $\text{MnBi}_2\text{Te}_4$ ,[14, 15], they were not observed in pure  $\text{MnBi}_2\text{Te}_4$  in the many magneto-transport studies up to 15 T[16–21], except for the report of small resistance oscillations [22]. This absence of SdHO in pure  $\text{MnBi}_2\text{Te}_4$  is most probably due to a low mobility caused by the strong disorder in the bulk, attributed mainly to Mn/Bi antisites [23–28], thus requiring very high magnetic fields to observe SdHO.

Here, we report magnetotransport measurements in Hallbar nanostructures of exfoliated  $\text{MnBi}_2\text{Te}_4$  up to very high magnetic fields (55 T) for the first time, revealing the clear signature of SdHO above 40 T. From the detailed study of their temperature and angular dependence, we identify the 2D nature of the electronic band responsible for these SdHO. By comparing the band-specific SdHO carrier density to the average carrier density extracted from the Hall effect, we determine the band bending of the bulk band at the top surface of the nanostructure. This study provides the first transport evidence of surface states in magnetic topological insulators.

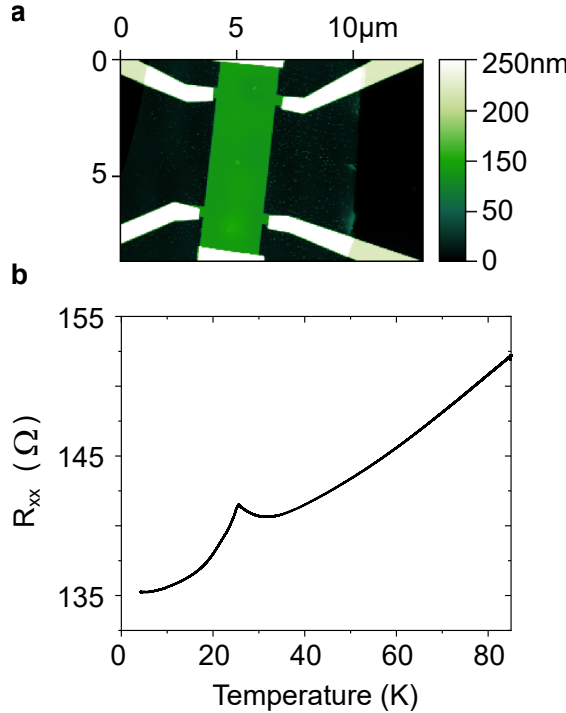


FIG. 1. **Device characterization.** a: Atomic force microscopy picture of an etched  $\text{MnBi}_2\text{Te}_4$  nanostructure, with thickness 91 nm and roughness of about 1 nm. The original shape of the  $\text{MnBi}_2\text{Te}_4$  exfoliated flake can still be faintly seen below the contacts. b: temperature dependence of the longitudinal resistance in zero magnetic field. The antiferromagnetic transition induces a resistance peak at 25.5 K.

Our samples consist of  $\text{MnBi}_2\text{Te}_4$  flakes exfoliated out of high-quality  $\text{MnBi}_2\text{Te}_4$  single crystals grown by controlled, slow cooling of a stoichiometric melt as reported in [23, 28]. The quality of the bulk crystals was confirmed by X-ray single-crystal diffraction and energy dispersive X-ray spectroscopy. The exfoliated flakes were then patterned using e-beam lithography to make ohmic Ti/Au contacts and a  $\text{TiO}_2$  hard mask to etch a Hall bar. We investigated two devices that yielded very similar results, as shown in Supplementary Information. An atomic force microscopy picture of one such device is presented in Fig.1a. The flake's thickness is 91 nm, with a low surface roughness of about 1 nm. The temperature dependence of the longitudinal resistance shows a dirty-metal behavior (low residual resistance ratio), with a pronounced resistance peak at 25.5 K at the antiferromagnetic Néel transition temperature  $T_N$ .

Fig.2 presents the longitudinal and the transverse magnetoresistance under perpendicular magnetic fields up to 55 T. At low field, both samples show the expected signature of a collinear antiferromagnet with a uniaxial anisotropy: a sharp resistance peak at about 3.1 T corresponds to the spin-flop magnetic transition,[29] which is also visible in the transverse resistance as a sharp jump

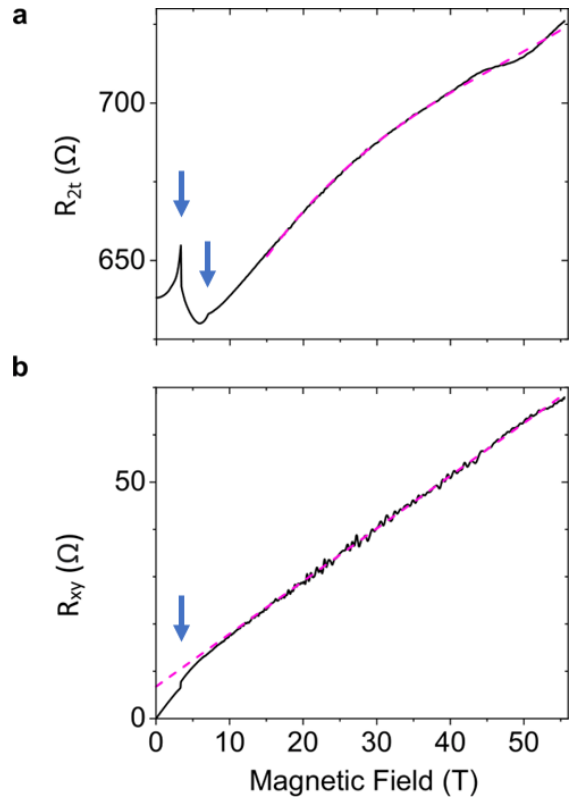


FIG. 2. **High-field magnetotransport in a  $\text{MnBi}_2\text{Te}_4$  nanostructure at 4.2 K.** a: Magnetoresistance and b: Hall effect up to 55 T. The magnetoresistance and Hall effect have been respectively symmetrized and antisymmetrized with magnetic field. Shubnikov-de-Haas oscillations are visible above about 40 T. Purple dashed lines represent respectively a cubic fit of the magnetoresistance, used afterward to extract Shubnikov-de-Haas oscillations, and a linear fit of the Hall effect asymptote at high field. Arrows indicate the spin-flop- and saturation fields.

of the anomalous Hall effect (blue arrows). Another feature is observed at 7 T, corresponding to the saturation field above which the magnetization is uniform (see Supplementary Information). Above 10 T, the transverse resistance is linear up to 55 T, corresponding to an asymptote of the normal Hall effect, yielding a total bulk carrier density of  $6.7 \times 10^{19} \text{ cm}^{-3}$ .

Above 40 T, oscillations appear in the longitudinal magnetoresistance. While only one and a half full oscillations are visible, those appear periodic in inverse magnetic field, as can be seen on Fig.3a. Their amplitude increases with the magnetic field, and they are damped by increasing temperature while remaining at the same position in field. We therefore identify them as Shubnikov-de-Haas oscillations. The appearance of SdHO at such high field reflects the moderate quantum mobility of the carriers, about  $250 \text{ cm}^2/\text{V.s}$ . The periodicity in inverse magnetic field of  $0.003 \text{ T}^{-1}$  corresponds to a magnetic frequency  $f_B = 167 \text{ T}$ ,

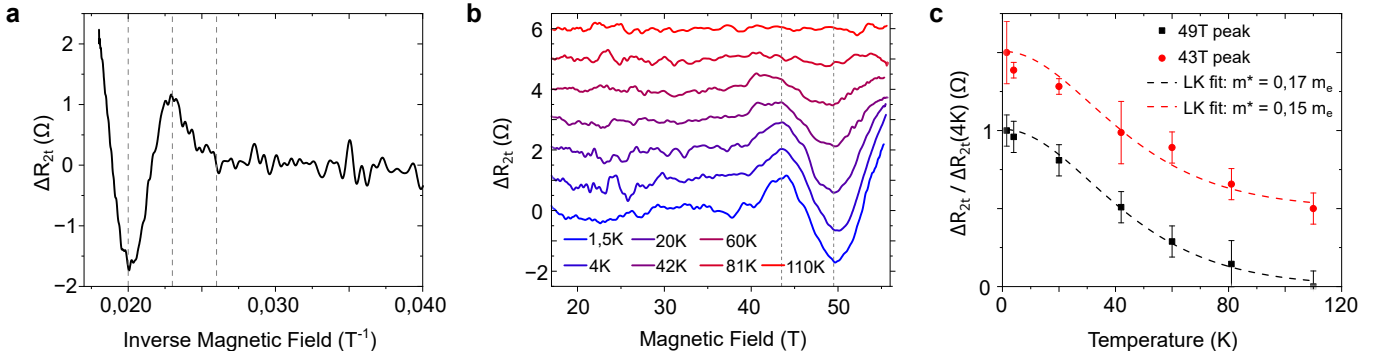


FIG. 3. **Temperature dependence of Shubnikov-de-Haas oscillations.** **a:** Residual Shubnikov-de-Haas oscillations after removal of a cubic background, versus inverse magnetic field. The dashed lines show the position of the SdHO extrema, separated by  $0.003 T^{-1}$ . **b:** Residual Shubnikov-de-Haas oscillations after removal of a cubic background, at different temperatures. The position of the minimum and maximum of the oscillation are indicated by dashed lines. **c:** Temperature dependence of the Shubnikov-de-Haas oscillation amplitude for the peaks at 43 and 49T. The error bars correspond to rapid noise in the raw data. Lifshitz-Kosevich fits lead effective masses  $m^*$  of about  $0.15 - 0.17 m_e$ .

a parameter directly related to the subband carrier density. We investigate the temperature dependence of the oscillations after removal of a monotonic background for each temperature, as shown in Fig.3b. The oscillations are slowly damped by increasing temperature, until they disappear at around 110 K. From this temperature dependence, we extract the effective mass  $m^*$  of the corresponding charge carriers through a Lifshitz-Kosevich fit (see Fig.3c).[30] The obtained value is  $m^* = 0.16 \pm 0.01 m_e$ , which could be compatible with both bulk states (close to  $0.15 m_e$ : the effective mass of the second bulk conduction band CB2, but significantly different from the other two bulk bands, see below and [31]) or with topological surface states with linear energy dispersion (for which  $m^* = E_F/v_F^2$ , with  $E_F$  and  $v_F$  the Fermi energy and Fermi velocity).

In order to determine the 3D or 2D character of the electronic population responsible for the observed SdHO, the magnetic field was tilted out of the sample plane by an angle  $\theta$ . From the angular dependence of the magnetoresistance we observe that the SdHO evolves with the angle, but is stable with respect to  $B_\perp = B \cos(\theta)$ . Fig.4a shows the SdHO plotted against the perpendicular component of the magnetic field  $B_\perp$ . The position of the maximum and minimum of the visible SdHO remains unaffected, while the positions vary with regard to the total field. This is a clear sign that the SdHO originate from a 2D electronic state in the sample plane. This is also compatible with the carrier density extracted from the SdHO frequency: if interpreted as a 3D parabolic bulk band, a magnetic frequency  $f_B = 167$  T corresponds to a bulk carrier density of  $n_{3D}^{SdHO} = 1/2\pi^2 (2e/h \times f_B)^{3/2} = 8 \times 10^{17} \text{ cm}^{-3}$ , which is two orders of magnitude smaller than the total carrier density extracted from the Hall effect. Interpreting the SdHO as originating from a topological surface state

(TSS) with linear energy dispersion and a Fermi velocity  $v_F = 5.5 \times 10^5 \text{ m.s}^{-1}$ ,[32, 33] we calculate a 2D carrier density of  $n_{2D}^{SdHO} = e/h \times f_B = 4.1 \times 10^{12} \text{ cm}^{-2}$  at the topological surface state, and a Fermi energy 255 meV above the Dirac point in good agreement with ARPES [34, 35].

In order to determine whether the surface state was localized on the top or the bottom surface of the nanostructure, we measured the dependence of the SdHO while applying a back-gate voltage (see Supplementary Information). As a large back-gate voltage of 110V did not induce any change on the SdHO, we conclude that the surface state responsible for the observed SdHO is not located on the bottom surface, but rather on the top one. The reason for the absence of visibility of SdHO originating from a bottom surface state probably lies in a lower mobility, which could be due to interaction with charge traps in the  $\text{SiO}_2$  substrate.

Consequently, we draw a model of the band filling and band bending in the nanostructure. This model, based on the density functional theory (DFT) calculations from [31], is summarized in Fig.4b and detailed below. DFT predicts three conduction bands in the bulk centered on the  $\Gamma$  point, CB1; CB2 and CB3, with respective effective masses  $0.09 m_e$ ,  $0.15 m_e$  and  $3 m_e$ , and bottom band energies at 80 meV and 310 meV below CB3 [31]. We use this simplified model of the bulk band structure to calculate the energy profile of the nanostructure at the bulk and surface. In this simple calculation, the bands are supposed perfectly parabolic and isotropic.

Since the carrier density of a 91 nm thick nanostructure is likely to be dominated by the bulk, we calculate the bulk carrier density as the total carrier density extracted from high-field Hall slope:  $n_{3D}^{\text{Hall}} = 6.7 \times 10^{19} \text{ cm}^{-3}$ . In the 3-bulk-band model, this corresponds to a bulk Fermi level about 317 meV above the bottom of the conduction band CB1 (see Supplementary Information). The bulk

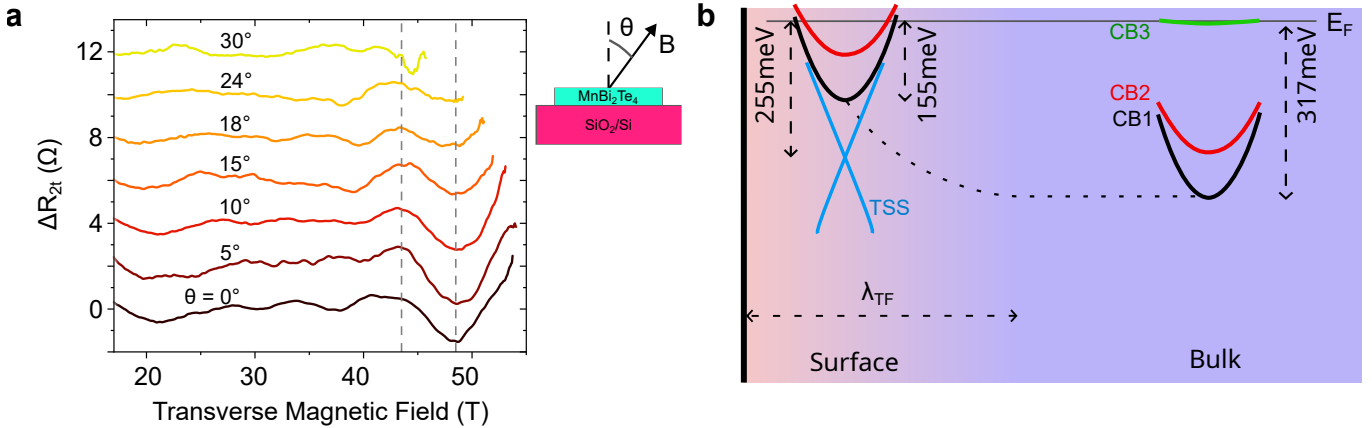


FIG. 4. **Angular dependence of Shubnikov-de-Haas oscillations and band bending.** **a:** Angular dependence of the Shubnikov-de-Haas oscillations after removal of a cubic background, between  $0^\circ$  (transverse field configuration) to  $30^\circ$  tilt toward in-plane configuration, shown against the transverse magnetic field component  $B_\perp$ . Curves shifted for clarity. The schematic shows the tilting angle  $\theta$  of the magnetic field. **b:** Schematic of the energy levels and band bending in the  $\text{MnBi}_2\text{Te}_4$  nanostructure, as extracted from Shubnikov-de-Haas and Hall data (see main text), in a model with three conduction bands (CB1, CB2, CB3, see main text) and one topological surface state (TSS).

chemical potential is therefore pinned at the bottom of the very heavy third conduction band CB3. While using a more exact model based on integrated density of states from DFT would change the exact value of the calculated bulk chemical potential, we argue that given the very large carrier density measured, the main result of the model - the very large bulk chemical potential - would not change qualitatively.

According to ARPES measurements on  $\text{MnBi}_2\text{Te}_4$ , the Dirac point lies about 100 meV below the bottom of the lowest conduction band CB1,[35–37], which, together with the  $E_F$  of 255 meV above the Dirac point as calculated above, results in an upward band bending of more than 150 meV between bulk (CB1 minimum at 317 meV) and surface (CB1 minimum at 155 meV). This upward band bending is a common situation in heavily doped 3DTI [38], where topological surface states are filled by charge transfer from heavily doped bulk bands, resulting in a lower doping of the bulk band close to the topological surface over the length-scale of the Thomas-Fermi screening length. It is, however, interesting to notice that, given the important band bending between TSS and bulk states, surface-sensitive techniques such as ARPES measurements would significantly underestimate the bulk chemical potential, and in particular the filling of the third conduction band CB3. Given the large effective mass of CB3, the bulk chemical potential will efficiently be pinned at the bottom of CB3 for carrier densities larger than  $\sim 5 \times 10^{19} \text{ cm}^{-3}$ .

We can further check the self-consistency of our model by calculating the effective mass expected for such topological surface states with such a Fermi energy. Using  $m^* = E_F/v_F^2$ , we obtain  $m^* = 0.148m_e$ , which is very close to the value extracted from the SdHO tempera-

ture dependence. This further confirms the 2D character of our SdHO. For TSS, the electronic mean free path is  $l_e = \mu m^* v_F/e = \mu E_F/e v_F$ . Considering the quantum mobility  $\mu = 1/(40 \text{ T}) = 250 \text{ cm}^2/\text{V.s}$  from the SdHO onset, this gives a lower estimate of the electronic mean free path  $l_e \simeq 11 \text{ nm}$ . This is lower than the value measured in non-magnetic TIs like  $\text{Bi}_2\text{Se}_3$  (21 nm, [6]), which is consistent with the higher doping level of  $\text{MnBi}_2\text{Te}_4$  as well as with the stronger chemical disorder, as due to cation intermixing.

In conclusion, we have studied magnetotransport up to very high magnetic fields in Hallbars of exfoliated  $\text{MnBi}_2\text{Te}_4$ . Above 40 T we evidence clear Shubnikov-de-Haas oscillations, due to the moderate mobility of the charge carriers in  $\text{MnBi}_2\text{Te}_4$ . The angular dependence of the Shubnikov-de-Haas oscillations in tilted field reveals their 2D origin. From Shubnikov-de-Haas and Hall effect analysis we construct a model of band bending in our nanostructure, yielding properties of both bulk- and surface states. Our study presents the first transport evidence of surface states in  $\text{MnBi}_2\text{Te}_4$ , which should play an important role in determining the transport properties in thin nanostructures. In particular, understanding and controlling the properties of the topological surface states is important to optimize the quantum anomalous Hall effect in magnetic topological insulators.

**Supporting Information** Additional magnetotransport data on both  $\text{MnBi}_2\text{Te}_4$  devices, including gate-, angle- and field dependencies (PDF)

**Acknowledgements** This work was supported by the Deutsche Forschungsgemeinschaft (DFG, German Research Foundation) under Germany's Excellence

Strategy through the Würzburg-Dresden Cluster of Excellence on Complexity and Topology in Quantum Matter – *ct.qmat* (EXC 2147, 0242021). LV was supported and by the French ANR (project number ANR-23-CPJ1-0158-01 and ANR-24-CE92-0021-01). L.V. and J. D. were supported by the Leibniz Association through the Leibniz Competition. This work was supported by the European Union’s H2020 FET Proactive project TOCHA (No. 824140), as well as by the CNRS International Research Project “CITRON”. We acknowledge the support of LNCMI-CNRS, a member of the European Magnetic Field Laboratory (EMFL) under proposal TMA01-222.

---

[1] D. J. Thouless, M. Kohmoto, M. P. Nightingale, and M. den Nijs, Quantized Hall Conductance in a Two-Dimensional Periodic Potential, *Phys. Rev. Lett.* **49**, 405 (1982).

[2] M. Z. Hasan and C. L. Kane, Colloquium: Topological insulators, *Reviews of Modern Physics* **82**, 3045 (2010).

[3] Y. Tokura, K. Yasuda, and A. Tsukazaki, Magnetic topological insulators, *Nature Reviews Physics* **1**, 126–143 (2019).

[4] A. R. Mellnik, J. S. Lee, A. Richardella, J. L. Grab, P. J. Mintun, M. H. Fischer, A. Vaezi, A. Manchon, E.-A. Kim, N. Samarth, and D. C. Ralph, Spin-transfer torque generated by a topological insulator, *Nature* **511**, 449 (2014).

[5] J.-C. Rojas-Sánchez, S. Oyarzún, Y. Fu, A. Marty, C. Vergnaud, S. Gambarelli, L. Vila, M. Jamet, Y. Ohtsubo, A. Taleb-Ibrahimi, P. Le Fèvre, F. Bertran, N. Reyren, J.-M. George, and A. Fert, Spin to Charge Conversion at Room Temperature by Spin Pumping into a New Type of Topological Insulator:  $\alpha$ -Sn Films, *Phys. Rev. Lett.* **116**, 096602 (2016).

[6] J. Dufouleur, L. Veyrat, B. Dassonneville, C. Nowka, S. Hampel, P. Leksin, B. Eichler, O. G. Schmidt, B. Büchner, and R. Giraud, Enhanced Mobility of Spin-Helical Dirac Fermions in Disordered 3D Topological Insulators, *Nano Letters* **16**, 6733 (2016).

[7] J. Dufouleur, L. Veyrat, A. Teichgräber, S. Neuhaus, C. Nowka, S. Hampel, J. Cayssol, J. Schumann, B. Eichler, O. G. Schmidt, B. Büchner, and R. Giraud, Quasiballistic Transport of Dirac Fermions in a  $\text{Bi}_2\text{Se}_3$  Nanowire, *Phys. Rev. Lett.* **110**, 186806 (2013).

[8] J. Dufouleur, L. Veyrat, B. Dassonneville, E. Xypakis, J. H. Bardarson, C. Nowka, S. Hampel, J. Schumann, B. Eichler, O. G. Schmidt, B. Büchner, and R. Giraud, Weakly-coupled quasi-1D helical modes in disordered 3D topological insulator quantum wires, *Scientific Reports* **7**, 45276 (2017).

[9] J. Dufouleur, E. Xypakis, B. Büchner, R. Giraud, and J. H. Bardarson, Suppression of scattering in quantum confined 2D helical Dirac systems, *Phys. Rev. B* **97**, 075401 (2018).

[10] C.-Z. Chang, C.-X. Liu, and A. H. Macdonald, Colloquium: Quantum anomalous Hall effect, *Rev. Mod. Phys.* **95**, 011002 (2023).

[11] D. K. Patel, K. M. Fijalkowski, M. Kruskopf, N. Liu, M. Götz, E. Pesel, M. Jaime, M. Klement, S. Schreyeck, K. Brunner, C. Gould, L. W. Molenkamp, and H. Scherer, A zero external magnetic field quantum standard of resistance at the 10–9 level, *Nature Electronics* **7**, 1111 (2024).

[12] W. Poirier and S. Djordjevic, A universal quantum electrical standard is getting closer, *Nature Electronics* **8**, 632 (2025).

[13] I. T. Rosen, M. P. Andersen, L. K. Rodenbach, L. Tai, P. Zhang, K. L. Wang, M. A. Kastner, and D. Goldhaber-Gordon, Measured Potential Profile in a Quantum Anomalous Hall System Suggests Bulk-Dominated Current Flow, *Phys. Rev. Lett.* **129**, 246602 (2022).

[14] Q. Jiang, C. Wang, P. Malinowski, Z. Liu, Y. Shi, Z. Lin, Z. Fei, T. Song, D. Graf, S. Chikara, X. Xu, J. Yan, D. Xiao, and J.-H. Chu, Quantum oscillations in the field-induced ferromagnetic state of  $\text{MnBi}_{2-x}\text{Sb}_x\text{Te}_4$ , *Phys. Rev. B* **103**, 205111 (2021).

[15] S. H. Lee, D. Graf, L. Min, Y. Zhu, H. Yi, S. Ciocey, Y. Wang, E. S. Choi, R. Basnet, A. Fereidouni, A. Wegner, Y. F. Zhao, K. Verlinde, J. He, R. Redwing, V. Gopalan, H. O. Churchill, A. Lanzara, N. Samarth, C. Z. Chang, J. Hu, and Z. Q. Mao, Evidence for a Magnetic-Field-Induced Ideal Type-II Weyl State in Antiferromagnetic Topological Insulator  $\text{Mn}(\text{Bi}_{1-x}\text{Sb}_x)_2\text{Te}_4$ , *Phys. Rev. X* **11**, 031032 (2021).

[16] J. Cui, M. Shi, H. Wang, F. Yu, T. Wu, X. Luo, J. Ying, and X. Chen, Transport properties of thin flakes of the antiferromagnetic topological insulator  $\text{MnBi}_2\text{Te}_4$ , *Phys. Rev. B* **99**, 155125 (2019).

[17] S. H. Lee, Y. Zhu, Y. Wang, L. Miao, T. Pillsbury, H. Yi, S. Kempinger, J. Hu, C. A. Heikes, P. Quarterman, W. Ratcliff, J. A. Borchers, H. Zhang, X. Ke, D. Graf, N. Alem, C.-Z. Chang, N. Samarth, and Z. Mao, Spin scattering and noncollinear spin structure-induced intrinsic anomalous Hall effect in antiferromagnetic topological insulator  $\text{MnBi}_2\text{Te}_4$ , *Phys. Rev. Res.* **1**, 012011 (2019).

[18] B. Chen, F. Fei, D. Zhang, B. Zhang, W. Liu, S. Zhang, P. Wang, B. Wei, Y. Zhang, Z. Zuo, J. Guo, Q. Liu, Z. Wang, X. Wu, J. Zong, X. Xie, W. Chen, Z. Sun, S. Wang, Y. Zhang, M. Zhang, X. Wang, F. Song, H. Zhang, D. Shen, and B. Wang, Intrinsic magnetic topological insulator phases in the Sb doped  $\text{MnBi}_2\text{Te}_4$  bulks and thin flakes, *Nature Communications* **10**, 4469 (2019).

[19] S.-K. Bac, K. Koller, F. Lux, J. Wang, L. Riney, K. Borisiak, W. Powers, M. Zhukovskyi, T. Orlova, M. Dobrowolska, J. K. Furdyna, N. R. Dilley, L. P. Rokhinson, Y. Mokrousov, R. J. McQueeney, O. Heinonen, X. Liu, and B. A. Assaf, Topological response of the anomalous Hall effect in  $\text{MnBi}_2\text{Te}_4$  due to magnetic canting, *npj Quantum Materials* **7** (2022).

[20] M. Martini, T. Confalone, Y. Lee, B. Rubrecht, G. Serrico, S. Shokri, C. N. Saggau, D. Montemurro, V. M. Vinokur, A. Isaeva, K. Nielsch, and N. Poccia, Hall effect in the  $\text{MnBi}_2\text{Te}_4$  crystal using silicon nitride nanomembrane via contacts, *Applied Physics Letters* **123**, 223102 (2023).

[21] L. Cao, Y.-Y. Lv, Y.-C. Luo, Y.-Y. Zhang, S. H. Yao, J. Zhou, Y. B. Chen, and Y.-F. Chen, The delicate coupling between magnetism and magneto-transport in Fermi-energy-adjusted  $\text{MnBi}_2\text{Te}_4$  crystals, *Applied Physics Letters* **125**, 063101 (2024).

[22] X. Lei, L. Zhou, Z. Hao, H. Liu, S. Yang, H. Sun, X. Ma, C. Ma, L. Wang, H.-Z. Lu, J.-W. Mei, J. Wang, and H. He, Magnetically tunable Shubnikov-de Haas oscillations in the  $\text{MnBi}_{2-x}\text{Sb}_x\text{Te}_4$  system, *Applied Physics Letters* **125**, 063102 (2024).

tions in  $\text{MnBi}_2\text{Te}_4$ , *Phys. Rev. B* **105**, 155402 (2022).

[23] M. M. Otrokov, I. I. Klimovskikh, H. Bentmann, D. Estyunin, A. Zeugner, Z. S. Aliev, S. Gaß, A. U. Wolter, A. V. Koroleva, A. M. Shikin, M. Blanco-Rey, M. Hoffmann, I. P. Rusinov, A. Y. Vyazovskaya, S. V. Ereameev, Y. M. Koroteev, V. M. Kuznetsov, F. Freyse, J. Sánchez-Barriga, I. R. Amiraslanov, M. B. Babanly, N. T. Mamedov, N. A. Abdullayev, V. N. Zverev, A. Alfonsov, V. Kataev, B. Büchner, E. F. Schwier, S. Kumar, A. Kimura, L. Petaccia, G. Di Santo, R. C. Vidal, S. Schatz, K. Kißner, M. Ünzelmann, C. H. Min, S. Moser, T. R. Peixoto, F. Reinert, A. Ernst, P. M. Echenique, A. Isaeva, and E. V. Chulkov, Prediction and observation of an antiferromagnetic topological insulator, *Nature* **576**, 416 (2019).

[24] J. Q. Yan, Q. Zhang, T. Heitmann, Z. Huang, K. Y. Chen, J. G. Cheng, W. Wu, D. Vaknin, B. C. Sales, and R. J. McQueeney, Crystal growth and magnetic structure of  $\text{MnBi}_2\text{Te}_4$ , *Phys. Rev. Mater.* **3**, 104409 (2019).

[25] C. Liu, Y. Wang, H. Li, Y. Wu, Y. Li, J. Li, K. He, Y. Xu, J. Zhang, and Y. Wang, Robust axion insulator and Chern insulator phases in a two-dimensional antiferromagnetic topological insulator, *Nature Materials* **19**, 522 (2020).

[26] S. Li, T. Liu, C. Liu, Y. Wang, H. Z. Lu, and X. C. Xie, Progress on the antiferromagnetic topological insulator  $\text{MnBi}_2\text{Te}_4$ , *National Science Review* **11**, 2024 (2024).

[27] D. Souchay, M. Nentwig, D. Günther, S. Keilholz, J. de Boor, A. Zeugner, A. Isaeva, M. Ruck, A. U. B. Wolter, B. Büchner, and O. Oeckler, Layered manganese bismuth tellurides with  $\text{GeBi}_4\text{Te}_7$ - and  $\text{GeBi}_6\text{Te}_{10}$ -type structures: towards multifunctional materials, *J. Mater. Chem. C* **7**, 9939 (2019).

[28] A. Zeugner, F. Nietschke, A. U. B. Wolter, S. Gaß, R. C. Vidal, T. R. F. Peixoto, D. Pohl, C. Damm, A. Lubk, R. Henrich, S. K. Moser, C. Fornari, C. H. Min, S. Schatz, K. Kißner, M. Ünzelmann, M. Kaiser, F. Scaravaggi, B. Rellinghaus, K. Nielsch, C. Hess, B. Büchner, F. Reinert, H. Bentmann, O. Oeckler, T. Doert, M. Ruck, and A. Isaeva, Chemical Aspects of the Candidate Antiferromagnetic Topological Insulator  $\text{MnBi}_2\text{Te}_4$ , *Chemistry of Materials* **31**, 2795 (2019).

[29] A. Tan, V. Labracherie, N. Kunchur, A. U. Wolter, J. Cornejo, J. Dufouleur, B. Büchner, A. Isaeva, and R. Giraud, Metamagnetism of Weakly Coupled Antiferromagnetic Topological Insulators, *Physical Review Letters* **124**, 197201 (2020).

[30] I. Lifshitz and A. Kosevich, Theory of magnetic susceptibility in metals at low temperatures, *Sov. Phys. JETP* **2**, 636 (1956).

[31] B. Xu, Y. Zhang, E. H. Alizade, Z. A. Jahangirli, F. Lyzwa, E. Sheveleva, P. Marsik, Y. K. Li, Y. G. Yao, Z. W. Wang, B. Shen, Y. M. Dai, V. Kataev, M. M. Otrokov, E. V. Chulkov, N. T. Mamedov, and C. Bernhard, Infrared study of the multiband low-energy excitations of the topological antiferromagnet  $\text{MnBi}_2\text{Te}_4$ , *Phys. Rev. B* **103**, L121103 (2021).

[32] L. Tomarchio, L. Mosesso, S. Macis, A. Grilli, M. Romani, M. C. Guidi, K. Zhu, X. Feng, M. Zacchigna, M. Petrarca, K. He, and S. Lupi, Electrodynamics of  $\text{MnBi}_2\text{Te}_4$  intrinsic magnetic topological insulators, *NPG Asia Materials* **14** (2022).

[33] Y. Gong, J. Guo, J. Li, K. Zhu, M. Liao, X. Liu, Q. Zhang, L. Gu, L. Tang, X. Feng, D. Zhang, W. Li, C. Song, L. Wang, P. Yu, X. Chen, Y. Wang, H. Yao, W. Duan, Y. Xu, S.-C. Zhang, X. Ma, Q.-K. Xue, and K. He, Experimental Realization of an Intrinsic Magnetic Topological Insulator, *Chinese Physics Letters* **36**, 076801 (2019).

[34] R. Xu, L. Xu, Z. Liu, L. Yang, and Y. Chen, ARPES investigation of the electronic structure and its evolution in magnetic topological insulator  $\text{MnBi}_{2+2n}\text{Te}_{4+3n}$  family, *National Science Review* **11**, nwad313 (2024).

[35] D. A. Estyunin, I. I. Klimovskikh, A. M. Shikin, E. F. Schwier, M. M. Otrokov, A. Kimura, S. Kumar, S. O. Filnov, Z. S. Aliev, M. B. Babanly, and E. V. Chulkov, Signatures of temperature driven antiferromagnetic transition in the electronic structure of topological insulator  $\text{MnBi}_2\text{Te}_4$ , *APL Materials* **8**, 021105 (2020).

[36] H. Li, S.-Y. Gao, S.-F. Duan, Y.-F. Xu, K.-J. Zhu, S.-J. Tian, J.-C. Gao, W.-H. Fan, Z.-C. Rao, J.-R. Huang, J.-J. Li, D.-Y. Yan, Z.-T. Liu, W.-L. Liu, Y.-B. Huang, Y.-L. Li, Y. Liu, G.-B. Zhang, P. Zhang, T. Kondo, S. Shin, H.-C. Lei, Y.-G. Shi, W.-T. Zhang, H.-M. Weng, T. Qian, and H. Ding, Dirac Surface States in Intrinsic Magnetic Topological Insulators  $\text{EuSn}_2\text{As}_2$  and  $\text{MnBi}_{2n}\text{Te}_{3n+1}$ , *Phys. Rev. X* **9**, 041039 (2019).

[37] Y.-J. Hao, P. Liu, Y. Feng, X.-M. Ma, E. F. Schwier, M. Arita, S. Kumar, C. Hu, R. Lu, M. Zeng, Y. Wang, Z. Hao, H.-Y. Sun, K. Zhang, J. Mei, N. Ni, L. Wu, K. Shimada, C. Chen, Q. Liu, and C. Liu, Gapless Surface Dirac Cone in Antiferromagnetic Topological Insulator  $\text{MnBi}_2\text{Te}_4$ , *Phys. Rev. X* **9**, 041038 (2019).

[38] L. Veyrat, F. Iacovella, J. Dufouleur, C. Nowka, H. Funke, M. Yang, W. Escoffier, M. Goiran, B. Eichler, O. G. Schmidt, B. Büchner, S. Hampel, and R. Giraud, Band Bending Inversion in  $\text{Bi}_2\text{Se}_3$  Nanostructures, *Nano Letters* **15**, 7503 (2015).